Available online at www.sciencedirect.com
SCIENCE DIRECT
Journal of Power Sources 153 (2006) 354–359
JOURNAL OF POWER SOURCES
www.elsevier.com/locate/jpowsour

Short communication

Physical characteristics and rate performance of $(CF_x)_n$ $(0.33 < x < 0.66)$ in lithium batteries

P. Lam [a,b,*], R. Yazami [a,c]

[a] *CALTECH-CNRS, Pasadena, CA 91125, USA*
[b] *Quallion LLC, 12744 San Fernando Rd, Sylmar, CA 91342, USA*
[c] *CNRS-LEPMI UMR 5631 BP75, 38402 St Martin d'Heres, France*

Available online 27 June 2005

Abstract

Sub-fluorinated graphite fluorides $(CF_x)_n$ compounds, $0.33 < x < 0.63$ were prepared from natural graphite and characterized by TGA, SEM-EDX and XRD. Their cathode behavior in lithium batteries was investigated under different discharge rates and compared to commercial petroleum coke based $(CF)_n$. At low discharge rate, the energy density increases with the fluorine content x. However, at higher rates, sub-fluorinated compounds performed better than commercial $(CF)_n$. The result is discussed with relation to higher electrical conductivity of sub-fluorinated compounds.

Keywords: Graphite fluoride; Fluorinated carbon; Rate capability; Lithium batteries

1. Introduction

Since the pioneer work of Ruff et al. in 1934 [1] and of Rudorff et al. in 1947 [2], graphite is known to react with elemental fluorine at high temperatures to yield graphite fluoride compounds of general formula $(CF_x)_n$. Systematic studies on the fluorination reaction later showed that the resulting F/C ratio highly depends on the fluorination temperature, the fluorine partial pressure and other physical characteristics of the graphite precursor, including the degree of graphitization, grain size and specific surface area [3–9].

The crystal structure of graphite fluorides $(CF_x)_n$ compounds with $x > 0.5$ was investigated by several groups [10–18]. The Watanabe group first proposed two phases: a stage-1 $(CF_1)_n$ and a stage-2 $(CF_{0.5})_n$, also commonly referred to as $(C_2F)_n$ [7]. In stage-1 compounds, the fluorine is intercalated between each carbon layers to yield CFCF layers stacking, whereas in stage-2 according to their model, fluorine occupies every other layer with a stacking sequence of CCFCCF. The hexagonal symmetry is preserved in both $(CF_1)_n$ and $(CF_{0.5})_n$ phases. Theoretical crystal structure calculations were also carried out and different layers stacking sequences were compared from their total energy [11,12,14,17,18].

$(CF_x)_n$ compounds are generally non-stoichiometric with x varying between ~0 and ~1.3. For $x < 0.04$, fluorine is mainly present on the surface of the carbon particles [19]. For $0.5 \leq x \leq 1$, it was suggested that the material consists of a mixture of two phases, $(CF_{0.5})_n$ and $(CF_1)_n$. Over-stoichiometric compounds $(1 \leq x \leq \sim 1.3)$ consist of $(CF_1)_n$ with additional perfluorinated $-CF_2$ surface groups [13]. Surprisingly, although they have been reported in the literature [3,19,20], covalent type $(CF_x)_n$ materials with $x < 0.5$ have not been investigated in view of their crystal structure characterization. One possible reason of the focus on the fluorine-rich materials comes from their potential application as lubricants and as cathode materials for primary lithium batteries. In fact for the later application, the energy density of the battery, which is determined by its discharge time at a specific rate and voltage, is an increasing function of 'x'. The cell overall discharge reaction, first postulated by Wittingham [21], can be schematized by Eq. (1).

$$(CF_x)_n + xn\,\mathrm{Li} \rightarrow n\mathrm{C} + nx\,\mathrm{LiF} \quad (1)$$

* Corresponding author.
E-mail address: karenl@quallion.com (P. Lam).

0378-7753/$ – see front matter © 2005 Elsevier B.V. All rights reserved.
doi:10.1016/j.jpowsour.2005.05.022

Table 1
Theoretical specific capacity of $(CF_x)_n$ compounds used as cathode materials in lithium battery

x in $(CF_x)_n$	0.25	0.33	0.50	0.66	1.00
Theoretical capacity ($mAh\,g^{-1}$)	400	484	623	721	864

Thus, the theoretical specific discharge capacity Q_{th}, expressed in $mAh\,g^{-1}$, is given by Eq. (2).

$$Q_{th}(x) = \frac{xF}{3.6(12+19x)} \quad (2)$$

where F is the Faraday constant and 3.6 is a unit conversion constant. Table 1 displays the theoretical capacity of $(CF_x)_n$ materials with different stoichiometry.

It is interesting to note that even a low fluorine-containing $(CF_{0.25})_n$ compound yields higher theoretical specific capacity than MnO_2; i.e. $400\,mAh\,g^{-1}$ versus $308\,mAh\,g^{-1}$, respectively. Despite higher capacity of $(CF_x)_n$ $x > 0.25$, MnO_2 is the most widely used solid state cathode in primary lithium batteries. Two possible reasons could be behind this: (1) lower cost and; (2) higher rate capability. Nevertheless, Li/$(CF)_n$ batteries are known to achieve longer shelf life in the order of 15 years together with outstanding high temperature stability.

The limited high rate performance of Li/$(CF)_n$ batteries is most likely due to the poor electrical conductivity of the $(CF)_n$ material. In fact, the fluorination of graphite at high temperature (typically $350\,^{\circ}C \leq T \leq 650\,^{\circ}C$) induces a dramatic change in the carbon atoms stereo-chemical arrangement. The planar sp^2 hybridization in the parent graphite transforms into a three-dimensional sp^3 hybridization in $(CF_x)_n$. In the latter, the carbon hexagons are puckered mostly in the chair conformation, and perhaps in lesser extent in the boat conformation [2,7–9,11,12,14,16,18,22]. Electron localization in the C–F bond leads to a huge drop of the electrical conductivity from $\sim 1.7 \times 10^4\,S\,cm^{-1}$ in graphite to $\sim 10^{-14}\,S\,cm^{-1}$ in $(CF)_n$ [7]. To compensate for the low conductivity of $(CF)_n$ while preserving the high thermal stability and high discharge capacity, we prepared a series of $(CF_x)_n$ materials with $0.33 < x < 0.63$ and investigated their thermal behavior, their crystal structure and their cathode performances particularly under high discharge rates.

2. Experimental

2.1. The $(CF_x)_n$ materials

Four samples of $(CF_x)_n$ (A, B, C and D) were synthesized by direct fluorination method of a natural graphite powder from Madagascar at the CNRS and Clermont-Ferrand University Lab. (France). The average particle size for the precursor was 7.5 μm for samples A, B and D, whereas an average particle size of 4 μm was used for sample C. The fluorination temperature ranged from 375 to 400 °C, and was adjusted to obtain the desired F/C ratios. A battery grade carbon monofluoride (E) derived from a petroleum coke was obtained from Advance Research Chemicals Inc. (ARC, Tulsa, OK, USA). Table 2 summarizes the synthesis conditions used for each sample.

Table 2
Synthesis conditions for the $(CF_x)_n$ samples

Sample	A	B	C	D	E
Precursor	NG	NG	NG	NG	Coke
Particle size (μm)	∼7.5	∼7.5	∼4	∼7.5	∼15–30
Temperature (°C)	375	380	390	400	N/A
Duration (h)	17	32	20	80	N/A

2.2. Physical characterization

Scanning electron microscopy (SEM, JEOL instrument) was performed to observe the particles morphology and analyze their composition (EDX). Micrographs were taken at various magnifications ranging from 500× to 10,000×.

The sample chemical composition was obtained by several methods. For samples A–D, the weight uptake during the fluorination reaction was used to determine the F/C ratio. EDX spectrometry provided semi-quantitative analyses of carbon and fluorine elements for all samples. These measurements were acquired on the SEM JEOL instrument with a Li drifted Si crystal detector, at a working distance of 10 mm, and analyzed using an INCA software. Additional elemental analysis was performed for sample E by a carbonate fusion method at ARC.

The thermal stability of the material was investigated by thermogravimetric analysis (TGA) performed on a Perkin-Elmer Pyris Diamond instrument. The weight loss of the material under argon atmosphere was recorded while it was being heated at a rate of $5\,^{\circ}C\,min^{-1}$ between 25 and 900 °C.

X-ray diffractometry (XRD) measurements were performed on a Rigaku instrument with Cu Kα radiation. Silicon powder (∼5 wt.%) was mixed in all samples and used as an internal reference. The spectra obtained were fitted on Xpert Highscore software. The resulting profiles were used in combination with CefRef software [23] to determine the 'a' and 'c' crystal parameters of the hexagonal cell (P_{-6m2}) as proposed by Touhara et al. [7].

2.3. Electrochemical performance

Conventional 2032 coin cells were assembled to test the electrochemical performance of the $(CF_x)_n$ materials. The cathode was prepared by spreading a slurry of 5 g $(CF_x)_n$, 0.62 g carbon black and 0.56 g polytetrafluoroethylene (PTFE)-based binder on an aluminum substrate. The anode is a lithium metal disc, and the separator consisted of microporous polypropylene Celgard 2500 membrane. The dimensions of the cathode, anode and separator are 15, 16 and 17.5 mm, respectively. The C-rate calculation was based on that theoretical capacity. The electrolyte is 1.2 M $LiBF_4$

in PC/DME 3/7. Stainless steel spacers and a wave washer were used to maintain a good pressure inside the coin cell. The coin cells were discharged on an Arbin instrument by applying a constant current with a voltage cutoff of 1.5 V. The discharge rates range from 0.01 to 2.5 C, and they were performed at room temperature. A minimum of three cells were used for each test condition.

3. Results and discussion

3.1. Physical characterization

The scanning electron micrographs show particle sizes ranging from 2 to 10 μm while the observed particle size of the commercially available $(CF_1)_n$ ranges from 10 to 35 μm. In addition to the particle size, the morphology of the two groups of samples seems to differ. The sub-fluorinated $(CF_x)_n$ samples are very thin flakes while the carbon monofluoride are bulkier. This difference comes from the use of a natural graphite precursor for samples A, B, C and D, and a larger petroleum coke precursor for sample E. Due to the size distribution of the particles after fluorination, it is not possible to observe a difference between the 4 and the 7.5 μm particles used for samples C and A, B and D, respectively. SEM photos were taken with a 5000× magnification and are shown on Fig. 1a–e to illustrate the differences.

The weight uptake during the graphite materials fluorination was converted to an F/C ratio. The EDX results provide a semi-quantitative elemental analysis, which can also be converted into an F/C ratio. To compensate for the lack of precision in this method, the measurements were averaged over a minimum of five different areas of the sample. Table 3 summarizes the composition results obtained for each sample and method. The composition for samples A, B, C and D as determined by weight uptake and EDX measurement correlates quite closely. The composition of sample E as determined by carbonate fusion method is also exactly the same as the one found by EDX measurements. In the next sections, samples A, B, C, D and E will also be referred to as $CF_{0.33}$, $CF_{0.46}$, $CF_{0.52}$, $CF_{0.63}$ and $CF_{1.08}$, respectively.

The TGA traces of all samples are shown in Fig. 2. Overall, we find three steps. Below 400 °C, materials A–D are very stable as there is less than 1% observed weight loss. Between 400 and 600 °C, A–D samples undergo a quick weight loss. While the weight loss profile is the same for A–C, material D follows an even more sudden drop between 525 and 580 °C. Beyond 600 °C, there is no major weight loss observed until at least 900 °C. The weight only decreases slowly at a rate of less than 2% per degree. Material E has the same thermogram profile as material D, but is a little more thermally stable, as it only starts decomposing around 450 °C and stops around 630 °C. The thermal stability difference observed between $CF_{0.33}$, $CF_{0.46}$, $CF_{0.52}$, $CF_{0.63}$ and $CF_{1.08}$ could be due to many factors including crystallinity of the precursor, particle size, synthesis conditions affecting the F/C ratio and heat-treatment temperature [10,24]. Hence, it is difficult to compare all these samples together. However, $CF_{0.33}$, $CF_{0.46}$, $CF_{0.52}$ and $CF_{0.63}$ all use a natural graphite of similar crystallinity, yet, $CF_{0.63}$ is interestingly more stable. Table 4 summarizes the TGA results and points out a higher initial weight loss for $CF_{0.52}$. This may relate to the smaller particle size, and thus larger surface area, of the precursor. More surface adsorption effects cause a more important weight loss at lower temperatures. Note that this only affects the initial weight loss as the general weight loss profile is still the same.

XRD patterns show a combination of broad and sharp peaks, with intensity variations reflecting the difference in fluorination amount (Fig. 3). The sharper peaks originate from the un-fluorinated precursor (graphite for $CF_{0.33}$, $CF_{0.46}$, $CF_{0.52}$, $CF_{0.63}$ and coke for $CF_{1.08}$) and are most obvious in samples $CF_{0.33}$, $CF_{0.46}$ and $CF_{0.52}$. The strongest graphite peak (0 0 2) is observed at 26.5° with decreasing relative intensity with 'x'. The broad peaks corresponding to the fluorinated phase are found at around 10, 25 and 40–45° for samples $CF_{0.33}$–$CF_{0.63}$, and around 13, 26 and 41° for sample $CF_{1.08}$. Table 5 shows the 'a' and 'c' parameters obtained for the fluorinated phases assuming a hexagonal lattice structure. Due to peaks broadening after fluorination, the assignment of diffraction peaks to only one phase is questionable.

3.2. Electrochemical performances

The discharge profile of the Li/$(CF_x)_n$ cells is showed in Fig. 4. While the battery grade carbon monofluoride exhibits the characteristic plateau around 2.5 V, the discharge profiles

Table 3
Chemical composition determined by weight uptake (A–D), EDX (A–E) and carbonate fusion method (E)

Sample		A	B	C	D	E
F/C ratio	Weight gain	0.33	0.46	0.52	0.63	N/A
	EDX	0.36	0.47	0.60	0.67	1.08
	ARC					1.08

Table 4
Summary of the TGA results on the $(CF_x)_n$ powders

Sample		$CF_{0.33}$	$CF_{0.46}$	$CF_{0.52}$	$CF_{0.63}$	$CF_{1.08}$
Temperature after	1% wt. loss	380	374	328	393	426
	2% wt. loss	423	427	403	459	467
	3% wt. loss	443	448	433	485	485
Wt.% remaining at 800 °C		55.6	49.7	40.9	35.7	18.4

Table 5
Summary of a and c parameters of the hexagonal unit cell derived from XRD measurements

Sample	$CF_{0.33}$	$CF_{0.46}$	$CF_{0.52}$	$CF_{0.63}$	$CF_{1.08}$
a (Å)	2.54	2.54	2.54	2.54	2.54
c (Å)	16.65	16.55	16.20	16.65	12.70

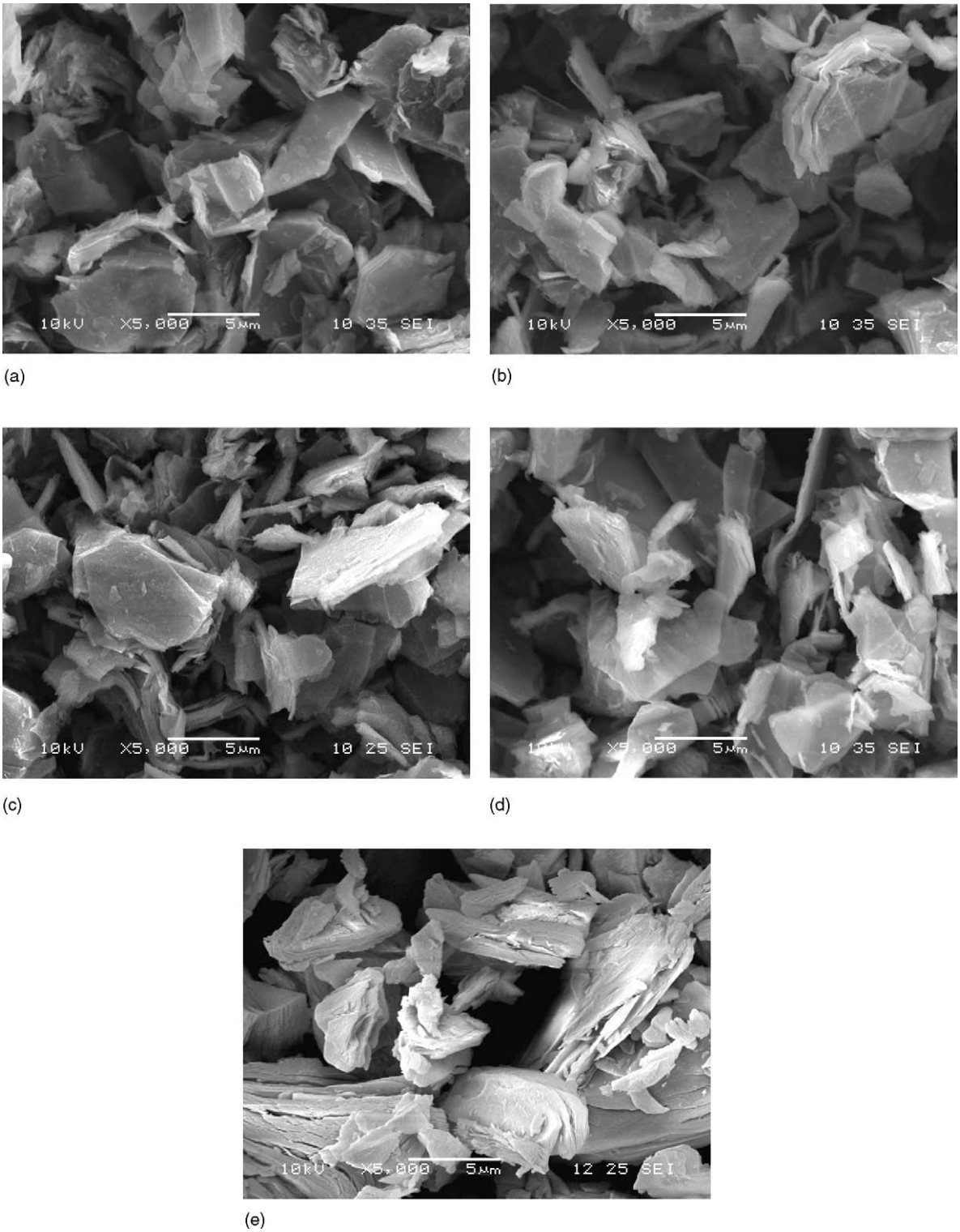

Fig. 1. Scanning electron micrographs of the $(CF_x)_n$ powders at a magnification of 5000×. (a) $x = 0.33$; (b) $x = 0.46$; (c) $x = 0.52$; (d) $x = 0.63$; and (e) $x = 1.08$.

of samples $CF_{0.33}$, $CF_{0.46}$ and $CF_{0.52}$ differ greatly in their voltage and shape. The discharge starts at a higher voltage of about ∼3 V, drops to about 2.8 V, slowly decreases to about 2.5 V, before a sharper drop to 1.5 V. The discharge curve of sample $CF_{0.63}$ falls in between the two previous groups. In the latter sample, the initial voltage is found at around 2.7 V; the slope of the curve is flatter than that of $CF_{0.33}$, $CF_{0.46}$ and $CF_{0.52}$, but steeper than $CF_{1.08}$. The discharge capacity

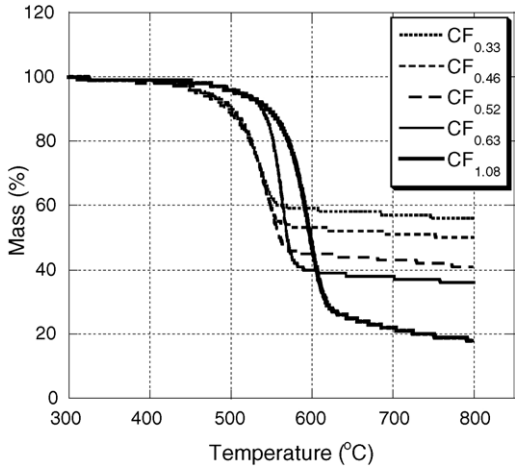

Fig. 2. TGA curves of the $(CF_x)_n$ powders at a rate of 5 °C min^{-1} in argon atmosphere.

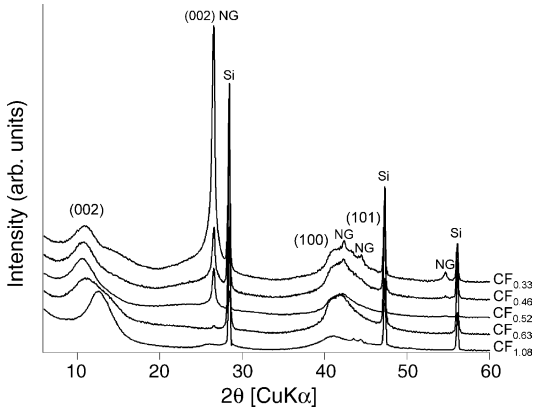

Fig. 3. XRD patterns of the $(CF_x)_n$ powders.

differs depending on the discharge rate and the F/C ratio. The variations in the potential are thought to come from the difference in the electrical conductivity of the material. Again, the existence of a unfluorinated graphitic phase

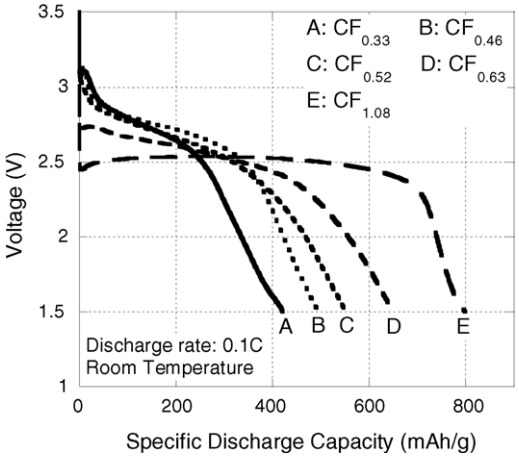

Fig. 4. Discharge profile of Li/$(CF_x)_n$ cells discharged at 0.1 C at RT.

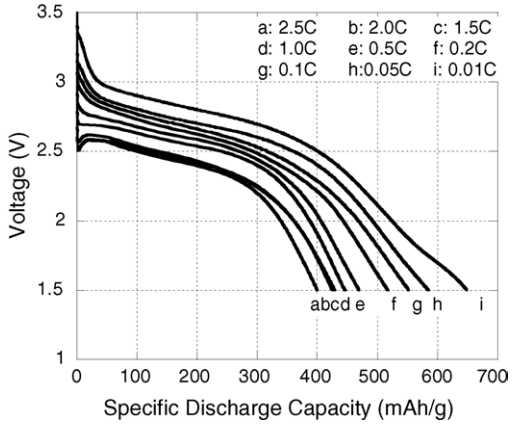

Fig. 5. Discharge profiles for Li/$CF_{0.52}$ coin cells discharged at different rates.

may result in a higher conductivity between the fluorinated grains of graphite fluoride, which reduces the cathodic over-potential. As a result, the lower the F/C, the higher the discharge voltage plateau.

For each material, the increase in the discharge current caused a decrease in the average discharge voltage and a reduced capacity. Fig. 5 illustrates the effect of the discharge rates on the discharge profile for sample $CF_{0.52}$. At the lowest discharge rates (C/100 to C/5), the voltage drops gradually from an open-circuit voltage of about 3.4 to 3 V. The initial voltage drop commonly observed in the fast discharges of Li/$(CF_x)_n$ batteries is only observed for rates of 1 C or higher in this specific example. The discharge curves corresponding to 1.5, 2 and 2.5 C are very similar in voltage and capacity, and exhibit a significant voltage drop at the beginning of discharge. Similar effects can be observed for the other materials (not shown here). Such a drop in the potential for higher discharge rate is associated to a steep increase in the over-potential at the higher discharge currents. Again, for the sub-fluorinated samples, the conductivity of the materials should be higher than that of the battery grade carbon monofluoride. As a result, the cell over-potential at high discharge rates is lower.

In order to compare the performance of the $(CF_x)_n$ materials under different discharge rates, a Ragone plot is presented in Fig. 6. It shows the achieved energy density $\mathcal{E}$ (Wh kg^{-1}) versus the power density $\mathcal{P}$ (W kg^{-1}) traces. $\mathcal{E}$ and $\mathcal{P}$ are determined from the discharge curves using Eqs. (3) and (4).

$$\mathcal{E} = \frac{q(i) \times < e_i >}{m} \tag{3}$$

$$\mathcal{P} = \frac{i \times < e_i >}{m} \tag{4}$$

where $q(i)$ and $< e_i >$ are, respectively, the discharge capacity (Ah) and the average discharge voltage (V) under current i (A) and m is the mass of active $(CF_x)_n$ in the electrode (kg). Note that the $\mathcal{P}$ scale in the Ragone plot is given as $\mathcal{P}^{1/2}$ for clarity purposes. As expected, carbon monofluo-

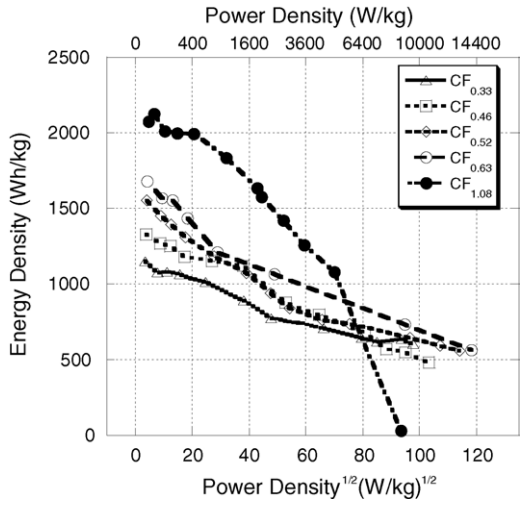

Fig. 6. Ragone plot comparing the performance of all Li/$(CF_x)_n$ cells.

ride has a very high energy density (over 2000 Wh kg^{-1}) for low rates of discharge (<C/10) while the sub-fluorinated graphites have significantly lower energy densities. Below 1000 W kg^{-1}, the energy density seems to be proportional to the F/C ratio of the materials. Beyond that point, the operating voltage and discharge capacity of carbon monofluoride are drastically reduced causing a large decrease in the energy density. Similarly, the capacity of materials A–D is also reduced; however, the operating voltage is still greater than that of sample E, and the energy density is greater than 500 Wh kg^{-1} over 2.5 C.

4. Conclusion

A series of graphite fluorides with F/C ratio ranging from 0.33 to 0.66 has been synthesized and their physical properties and electrochemical performance has been studied in a systematic manner and compared to commercial (CF_1) compound. For the first time, a complete analysis of the rate performance of this type of graphite fluorides has been performed. Despite the numerous benefits of using carbon monofluoride as a battery material, our results show that a partially fluorinated graphite fluorides could outperform the traditional fluorinated petroleum coke. The sub-fluorinated samples contained some un-reacted graphite, which could act as an intrinsic conductor between the graphite fluoride particles. Although lower fluorination content decreases the specific discharge capacity of the material, it increases the battery performance when discharged at very high rates. There is indeed a trade-off between fluorination content and high rate capability.

Acknowledgements

The authors would like to thank Prof. André Hamwi of Université de Clermont-Ferrand and CNRS (France) for synthesizing the graphite fluorides samples and Dr. Dayal Meshri of Advance Research Chemical (Tulsa, OK, USA) for providing the carbon monofluoride. They also acknowledge the technical support of scientists and engineers from Quallion LLC (Sylmar, CA, USA); Dr. Tracy Piao, Mr. Manabu Tanaka, Mr. Hiroyuki Yumoto for SEM, EDX and TG measurements. Thanks also to Prof. Brent Fultz of the California Institute of Technology and Dr. Hisashi Tsukamoto of Quallion LLC for their stimulating discussions.

References

[1] O. Ruff, O. Bretschneider, F. Elert, Z. Anorg. Allg. Chem. 217 (1934) 1.
[2] W. Rudorff, G. Rudorff, Z. Anorg, Allg. Chem. 253 (1947) 281.
[3] A.K. Kuriakos, J.L. Margrave, J. Phys. Chem. 69 (1965) 2272.
[4] G. Nanse, E. Papirer, P. Fioux, F. Moquet, A. Tressaud, Carbon 35 (1997) 175.
[5] A. Morita, T. Iijima, T. Fujii, H. Ogawa, J. Power Sources 5 (1980) 111.
[6] H. Fujimoto, Carbon 35 (1997) 1061.
[7] H. Touhara, K. Kadono, Y. Fujii, N. Watanabe, Z. Anorg. Allg. Chem. 544 (1987) 7.
[8] N. Watanabe, M. Takashima, K. Takahashi, Nippon Kagaku Kaishi 1033 (1974).
[9] Y. Kita, N. Watanabe, Y. Fujii, J. Am. Chem. Soc. 101 (1979) 3832.
[10] T. Nakajima, N. Watanabe, Graphites Fluorides and Carbon–Fluorine Compounds, CRC Press, Boca Raton, FL, 1991, p. 84.
[11] J.-C. Charlier, X. Gonze, J.-P. Michenaud, Mol. Cryst. Liq. Cryst. 244 (1994) 135.
[12] J.-C. Charlier, X. Gonze, J.-P. Michenaud, Phys. Rev. B 47 (1993) 162.
[13] V.N. Mitkin, I.P. Asanov, L.N. Mazalov, J. Struct. Chem. 43 (2002) 843.
[14] A. Zajac, P. Pelikan, J. Minar, J. NOga, M. Strada, P. Banacky, S. Biskupic, J. Sol. State Chem. 150 (2000) 286.
[15] V. Gupta, T. Nakajima, B. Zemva, J. Fluorine Chem. 110 (2001) 245.
[16] L.B. Ebert, J.I. Brauman, R.A. Huggins, J. Am. Chem. Soc. 96 (1974) 7841.
[17] P. Pelikan, J. Noga, S. Biskupic, J. Solid State Chem. 174 (2003) 233.
[18] L.G. Bulusheva, A.V. Okotrub, N.F. Yudanov, Phys. Low-Dim. Struct. 7/8 (2002) 1.
[19] T. Nakajima, M. Koh, R. Niwas, M. Shimada, Electrochem. Acta 44 (1999) 2879.
[20] J.L. Wood, R.B. Badachhape, R.J. Lagow, J.L. Margrave, Abs. Am. Chem. Soc. 121 (1973).
[21] M.S. Wittingham, J. Electrochem. Soc. 122 (1975) 526.
[22] R.J. Lagow, R.B. Badachhape, J.L. Wood, J.L. Margrave, J. Chem. Soc. Dalton Trans. 1268 (1974).
[23] http://www.ccp14.ac.uk/tutorial/lmgp/celref.htm.
[24] S. Koyama, Ph.D. thesis, Kyoto University, Japan, 1980.